Optimal sizing of energy storage systems under uncertain demand and generation

Optimal sizing of energy storage systems under uncertain demand and generation

Martina Bucciarelli[1], Simone Paoletti, Antonio Vicino

Dipartimento di Ingegneria dell'Informazione e Scienze Matematiche, Università di Siena, via Roma 56, Siena 53100, Italy

e-mail: {bucciarelli, paoletti, vicino}@diism.unisi.it

Abstract

Energy storage systems have been recently recognized as an effective solution to tackle power imbalances and voltage violations faced by distribution system operators due to the increasing penetration of low carbon technologies. To fully exploit their benefits, optimal sizing of these devices is a key problem at the planning stage. This paper considers the sizing problem of the energy storage systems installed in a distribution network with the aim of preventing over- and undervoltages. In order to accommodate uncertainty on future realizations of demand and generation, the optimal sizing problem is formulated in a two-stage stochastic framework, where the first stage decision involves the storage sizes, while the second stage problem ~~is a full AC optimal power flow providing~~ provides the optimal storage control policy for given demand and generation profiles. By taking a scenario-based approach, the two-stage problem is approximated in the form of a single multi-scenario, multi-period optimal power flow, whose size, however, becomes computationally intractable as the number of scenarios grows. To overcome this issue, the paper presents a procedure to compute upper- and lower bounds to the optimal cost of the approximated problem. Moreover, when the objective is to minimize the total installed storage capacity, an iterative algorithm based on scenario reduction is proposed, which converges to the optimal solution of the approximated problem. The whole procedure is tested on the topology of the IEEE 37-bus test network, considering scenarios of demand and generation which feature over- and undervoltages in the absence of storage devices.

Keywords: Energy storage sizing, distribution network, optimal power flow, scenario reduction, two-stage stochastic programming.

1. Introduction

The ever growing ~~uncoordinated~~ penetration of low carbon technologies, such as distributed generation (e.g., wind and photovoltaic), electric vehicles and heat pumps, is a matter of concern for distribution systems operators (DSOs), which have to guarantee a predefined level of quality for electricity supply. In particular, modifications of typical power flows in distribution networks may cause abnormal fluctuations of the voltage magnitude, which are not tolerated beyond specified limits around the nominal value. In this respect, energy storage systems (ESSs) have been recently recognized as an effective solution for DSOs to tackle voltage problems in distribution feeders [1], representing an alternative to other solutions, such as traditional grid reinforcement, on-load tap changers at secondary substations [2, 3], soft-open points [4], and reactive power control of distributed generation (DG) [5]. ESSs are storage devices interfaced with the grid through a power electronic converter. In this way, they can be controlled to act as loads in case of overvoltages, and as generators in case of undervoltages. This adds to a number of other benefits that ESSs bring to the whole electricity system, and to different stakeholders [6, 7, 8].

To fully exploit the benefits of storage devices, the problem of their optimal allocation must be addressed at the planning stage. The ESS allocation decision problem consists of defining the type and the number of devices to be deployed, their locations (siting), and sizes (sizing) [9]. The interested reader is referred to the survey paper [10] for a literature review on ESS allocation techniques, classified according to both the ESS application and the methodology used to find a solution. In most cases, optimal ESS siting and sizing are carried out simultaneously, either through a cost-benefit analysis [11, 12], or formulating a single optimization problem [13, 14, 15]. In other cases, the two problems are dealt with separately. A heuristic method is proposed in [16] to detect the sensitive buses of the grid under a wide range of contingencies. Voltage magnitudes and angles under the contingencies are forecast by exploiting complex-valued neural networks and time domain power flow. In [17], the ESS siting prob-

[1]Corresponding author.

Nomenclature

Acronyms

AC	Alternating current
DC	Direct current
DG	Distributed generation
DSO	Distribution system operator
ESS	Energy storage system
LV	Low voltage
MV	Medium voltage
OPF	Optimal power flow
PF	Power flow
SDP	Semidefinite programming

Parameters

ΔT	Time step
T	Number of time steps per day
η_s^c, η_s^d	Charging and discharging efficiencies of storage at bus s
$\Gamma_s, \Upsilon_s, \Xi_s$	Column vectors of the polygonal approximation of the capability curve of the storage at bus s
ρ_s	Power-to-energy ratio of the storage at bus s
$\underline{E}_s$	Lower limit of the energy level of the storage at bus s
$\overline{S}_{ij}$	Upper bound on the apparent power through line (i,j)
$\overline{v}_i$	Upper bound on the voltage magnitude at bus i
$\underline{v}_i$	Lower bound on the voltage magnitude at bus i
p_d	Scenario of demand and generation
π_d	Probability of scenario p_d
Y_{ij}	(i,j)-entry of the network admittance matrix Y
y_{ij}	Line admittance between buses i and j

Sets

$\mathcal{D}$	Index set of scenarios
$\mathcal{E}$	Set of lines
$\mathcal{L}$	Set of load buses
$\mathcal{N}$	Set of buses
$\mathcal{P}$	Set of scenarios
$\mathcal{S}$	Set of buses equipped with storage
$\mathcal{T}$	Set of time steps
$\mathcal{X}$	Feasible solution set for the first-stage problem
$\mathcal{Y}$	Feasible solution set for the second-stage problem

Variables

E_s	Energy capacity of the storage at bus s
$r_s(t)$	Active power exchanged by the storage at bus s at time t
$b_s(t)$	Reactive power exchanged by the storage at bus s at time t
$e_s(t)$	Energy level of the storage at bus s at time t
$P_i^D(t)$	Active power demanded at bus i at time t
$P_i^G(t)$	Active power generated at bus i at time t
$Q_i^D(t)$	Reactive power demanded at bus i at time t
$Q_i^G(t)$	Reactive power generated at bus i at time t
$S_i(t)$	Net complex power injection into bus i at time t
$V_i(t)$	Complex voltage at bus i at time t
x	Decision variables of the first-stage problem
y_d	Decision variables of the second-stage problem for scenario p_d

lem is tackled via a different heuristic approach, which returns the most suitable ESS locations in the grid based on voltage sensitivity analysis. In some applications, ESS locations may also be decided a priori, and the ESS allocation problem boils down to determine only the size of each ESS.

For given ESS type, number and locations, a quite general approach is to formulate the ESS sizing problem in an optimal power flow (OPF) framework, where a suitable cost function (typically including storage installation and operation costs, as well as power losses and generation costs) is optimized, subject to storage dynamics, power flow and network constraints. Linearization of power flow constraints via DC approximation is often adopted when dealing with transmission networks, where line resistances are typically negligible compared to line reactances [18, 19, 20]. When such an assumption is not valid, like in distribution networks, a full or approximated AC OPF is considered. Branch flow equations are used to model the power network in [13, 14, 21]. A bi-level optimization model, where the second-level problem is a linear program minimizing the daily coincident peak demand, is proposed in [15]. In [22], linear approximations for voltage, branch flow, and network power losses are presented, leading to a linearized OPF. A simplified power balance model of the network is adopted in [23], while in [24] the distribution network is modelled through a continuous tree with linearized DistFlow model. These simplified models are defined to cope with the computational burden of (multi-period) AC OPF problems, due to nonconvexity of AC power flow equations, and time-coupling constraints introduced by ESS dynamics. Other solution strategies proposed in the literature for the same purpose, rely on semidefinite convex relaxations of the OPF problem [25, 26, 27], second-order cone programming [13, 21], and alternating direction method of multipliers [14].

In deterministic OPF problems, net power injected at load buses is assumed to be given, but unfortunately future realizations of demand and DG are unknown at the planning stage. This calls for a formulation of the optimal ESS sizing problem which takes uncertainty sources explicitly into account. Stochastic optimization paradigms are suitable to this aim [28]. Probability density functions of wind power generation and demand are considered in [20, 29] within probabilistic OPF formulations. A two-stage programming formulation of the optimal ESS sizing problem is proposed in [23], including chance constraints to model wind forecast errors. Chance constraints

accounting for wind power and demand forecast errors, are also considered in [30]. Since stochastic optimization problems are typically intractable, they are often tackled by defining a large number of scenarios, which are expected to represent the original stochastic information. Suitable scenario generation techniques based on time-series and regression models [31], as well as copula models [32], can be used to this aim. An approximate reformulation of the optimization problem is derived by replicating power flow variables and constraints for each scenario [13, 14, 23]. In order to keep the problem size affordable, scenario-based approaches are often coupled with techniques to downsize the scenario set. To this aim, clustering algorithms such as K-means and centroid-linkage clustering, are adopted [13, 23]. Another possibility is to apply scenario reduction techniques based on the notion of probability distance [33]. However, as shown in [34], all these techniques may fail in preserving the information content useful to the solution of the original problem.

This paper addresses the optimal ESS sizing problem for an active distribution network, with the aim of preventing over- and undervoltages. This is done by taking the point of view of the DSO, and by including uncertainty on future demand and DG explicitly in the formulated decision problem. As the main paper contribution, a novel scenario reduction technique is proposed within a two-stage stochastic programming formulation of the ESS sizing problem. The distinctive feature of the proposed technique is that scenario reduction is accomplished by exploiting the structure of the optimization problem to be solved. This is expected to get better results compared to standard clustering methods, typically adopted in the literature on scenario-based approaches. In order to assess the expected improvement, a comparison with the classical scenario reduction technique [33], based on the notion of probability distance, is performed in the case study of Section 5.

The proposed approach to ESS sizing can be summarized according to the following steps.

i) The decision problem is formulated as a two-stage stochastic program, where the first stage decision involves the total installed storage capacity, while the second stage problem is a full AC OPF in the bus injection model, providing the optimal ESS control policy for given demand and DG profiles.

ii) By taking a scenario-based approach, the two-stage problem is approximated in the form of a multi-scenario, multi-period OPF. If, on the one hand, a very large number of scenarios is needed for an accurate approximation, on the other hand the size of the OPF becomes computationally intractable as the number of scenarios grows. To overcome this issue, a technique is proposed to derive a feasible solution of the multi-scenario problem by solving a single-scenario problem for each scenario. As an additional outcome of this procedure, a lower bound to the optimal cost of the multi-scenario problem is obtained, making it possible to evaluate the quality of any feasible solution found.

iii) For the case when the objective is to minimize the total installed storage capacity, an iterative procedure to solve the ESS sizing problem at the optimum is proposed. The procedure consists of a sequence of optimal ESS sizing problems with scenario sets of increasing size. The solutions of the downsized problems converge to the exact solution of the multi-scenario OPF typically after few iterations. The convergence property is a direct consequence of the proposed scenario reduction technique, which is based on a metric exploiting the structure of the multi-scenario problem.

The whole procedure is tested on the topology of the IEEE 37-bus test network, considering 100 scenarios of demand and DG which feature over- and undervoltages in the absence of ESSs. For this application, the multi-scenario OPF problem cannot be solved directly, while the proposed iterative algorithm is able to find the optimal solution after few iterations.

The paper is organized as follows. Section 2 presents the network model, the formulation of the two-stage optimal ESS sizing problem, and its scenario-based approximation. A feasible solution of the multi-scenario problem, as well as upper and lower bounds to its optimal cost, are derived in Section 3. Section 4 describes the scenario reduction-based iterative algorithm to solve the multi-scenario problem at the optimum, when the objective is to minimize the total installed ESS capacity. Finally, numerical results are illustrated in Section 5, and conclusions are drawn in Section 7. A preliminary version of this work appeared in the conference paper [35], where simplified models of the network and of the storage were considered, and an upper bound to the optimal cost of the multi-scenario problem was derived by finding a suitable feasible solution. Moreover, compared to [35], the case study worked out in this paper involves a more realistic test network of larger size.

2. Problem formulation

The bus injection model of a distribution network is summarized at the beginning of this section. Then, the constraints of the considered ESS sizing problem are described, and a problem formulation in the framework of two-stage stochastic programming is presented. By adopting a scenario-based approach, the two-stage problem is finally approximated with a multi-scenario, multi-period OPF.

In the following, $\mathrm{Re}(z)$, $\mathrm{Im}(z)$, $|z|$ and z^* denote the real part, imaginary part, modulus and complex conjugate of the complex number z, respectively. For a real number

x, $[x]^+ = \max\{x, 0\}$ and $[x]^- = \max\{0, -x\}$. Moreover, $u(t)$ is the value of the variable u at time $t\Delta T$, where $t = 1, 2, \ldots$ is the discrete time index, and ΔT is the time step.

2.1. Bus injection model

Together with the branch flow model, the bus injection model is one of the standard models used for power flow analysis and optimization [27]. The model involves nodal variables such as voltages and current/power injections. Let a distribution network be described by a graph $(\mathcal{N}, \mathcal{E})$, where $\mathcal{N} = \{1, 2, \ldots, n\}$ is the set of nodes (*buses*) and $\mathcal{E}$ is the set of edges (*lines*). According to the classical π-model for the n-bus system [36], the admittance-to-ground at bus i is denoted by y_{ii}, while $y_{ij} = y_{ji}$ is the line admittance between buses i and j. If $(i, j) \notin \mathcal{E}$, $y_{ij} = 0$. At time t, the complex voltage at bus i is denoted by $V_i(t)$, while the net complex power injection into bus i is denoted by $S_i(t)$. These quantities are related by the power balance equations

$$S_i(t) = V_i(t) \sum_{j \in \mathcal{N}} V_j^*(t) Y_{ij}^*, \tag{1}$$

where

$$Y_{ij} = \begin{cases} y_{ii} + \sum_{h \neq i} y_{ih} & \text{if } i = j \\ -y_{ij} & \text{otherwise.} \end{cases} \tag{2}$$

In the following, $P_i(t)$ will denote the real part of $S_i(t)$ in (1), namely

$$P_i(t) = \mathrm{Re}\left(V_i(t) \sum_{j \in \mathcal{N}} V_j^*(t) Y_{ij}^* \right). \tag{3}$$

Without loss of generality, it is assumed that bus 1 represents the interconnection with an external grid and, to the purpose of power flow (PF) studies, it is modelled as a *slack* bus with fixed complex voltage $V_1(t)$. The other buses in the set $\mathcal{L} = \{2, \ldots, n\}$ are modelled as *load* buses, for which the known quantities are the net complex power injections, namely $S_i(t)$ in (1). At time t and for given $V_1(t)$, $S_2(t)$, ..., $S_n(t)$, the PF problem consists of solving the system of nonlinear equations (1), $i \in \mathcal{N}$, with respect to the unknowns $S_1(t)$, $V_2(t)$, ..., $V_n(t)$. There are several methods for carrying out this task, the most popular being the Newton-Raphson method (see, e.g., [36, Chap. 3]).

2.2. Constraints

OPF problems are optimization problems where the power balance equations (1) appear among the constraints. Additional constraints are typically included to describe desired/physical limits on controllable and power flow variables.

2.2.1. ESS operation constraints

Let m be the number of ESSs. The subset of buses equipped with ESSs is denoted by $\mathcal{S} = \{s_1, \ldots, s_m\} \subseteq \mathcal{L}$. The energy level in the storage at bus s is denoted by $e_s(t)$, while $r_s(t)$ is the active power exchanged by the ESS at bus s. If power is injected into the ESS, then $r_s(t) > 0$, whereas $r_s(t) < 0$ when power is extracted from the ESS. With the same convention about the sign, the reactive power exchanged by the ESS at bus s is denoted by $b_s(t)$. The variables $e_s(t)$, $r_s(t)$ and $b_s(t)$ are constrained as follows:

$$e_s(t) = e_s(t-1) + \eta_s^c \left[r_s(t) \right]^+ \Delta T - \frac{1}{\eta_s^d} \left[r_s(t) \right]^- \Delta T \tag{4}$$

$$e_s(T) = e_s(0) \tag{5}$$

$$\underline{E}_s \leq e_s(t) \leq E_s \tag{6}$$

$$\Gamma_s \, r_s(t) + \Upsilon_s \, b_s(t) \leq \Xi_s E_s. \tag{7}$$

The first-order difference equation (4) models the dynamics of $e_s(t)$, where η_s^c and η_s^d are the charging and discharging efficiencies of the storage at bus s. The initial condition $e_s(0)$ is assumed to be given. Since in this paper a time horizon of one day is considered, the constraint that the storage energy level is equal at the beginning and at the end of the day, is imposed through (5), where T is the number of time steps per day. This is done in order to decouple ESS operation over different days. Constraint (6) states that the storage energy level at bus s cannot exceed its maximum capacity E_s, neither it can go below a given lower limit represented by $\underline{E}_s \geq 0$. The ESS capability curve is modelled by (7), which represents a polygonal approximation of the feasible region for the pair $\big(r_s(t), b_s(t)\big)$. Examples of the vectors Γ_s, Υ_s and Ξ_s are reported in Appendix A for the case of a regular polygon with an even number of sides. The right-hand side of (7) is a function of E_s to model the possible dependence of power ratings on energy ratings for a given storage technology [18]. It is worthwhile to note that the adopted storage technology enters the model through the coefficients η_s^c and η_s^d, and the vector Ξ_s.

2.2.2. Network operation constraints

Network operation constraints include power balance equations, and constraints on voltages and line power flows:

$$\mathrm{Re}\left(V_i(t) \sum_{j \in \mathcal{N}} V_j^*(t) Y_{ij}^* \right) = P_i^G(t) - P_i^D(t) - r_i(t) \tag{8}$$

$$\mathrm{Im}\left(V_i(t) \sum_{j \in \mathcal{N}} V_j^*(t) Y_{ij}^* \right) = Q_i^G(t) - Q_i^D(t) - b_i(t) \tag{9}$$

$$\underline{v}_i^2 \leq |V_i(t)|^2 \leq \overline{v}_i^2 \tag{10}$$

$$\left| V_i(t) \big[V_i(t) - V_j(t) \big]^* y_{ij}^* \right| \leq \overline{S}_{ij}. \tag{11}$$

For a generic bus $i \in \mathcal{L}$, possibly having loads, generators and ESS connected to it, the power balance equations (1) are rewritten in (8)-(9) by highlighting all active and reactive power contributions, where $P_i^G(t)$ and $P_i^D(t)$ denote the active power generated and demanded at bus i, and $Q_i^G(t)$ and $Q_i^D(t)$ have a similar meaning in terms of reactive power (all these quantities are assumed to be nonnegative). In (8)-(9), if no load, generator or ESS is

connected to bus i, the corresponding contribution is set equal to zero. Constraint (10) is enforced to keep the voltage magnitude between bounds imposed by voltage quality requirements, with $\underline{v}_i \leq \overline{v}_i$ given positive constants. Finally, physical properties of the lines impose a limit on the apparent power transferred from bus $i \in \mathcal{N}$ to the rest of the network through the line $(i,j) \in \mathcal{E}$. This limit is expressed by the constraint (11), where $\overline{S}_{ij} = \overline{S}_{ji}$ are given upper bounds.

2.3. ESS sizing via two-stage stochastic programming

The problem addressed in this paper consists of deciding the sizes E_s of the ESSs to be installed for voltage support in a distribution network. The number and the locations of the ESSs are therefore assumed to be given. The interested reader is referred to the survey paper [10] for a review of ESS siting techniques proposed in the literature. The ESS sizing procedure presented next can be embedded in the iterative ESS allocation scheme of [17].

The ESS sizing problem is formulated in the two-stage stochastic optimization framework of [28]. This choice is motivated by the fact that, at the planning stage, future realizations of demand and generation are unknown. Therefore, a problem setting which explicitly accounts for uncertainty, has to be considered. A two-stage stochastic program is a problem written in the form

$$\min_{x \in \mathcal{X}} \mathbb{E}_{\mathbf{p}}[G(x,\mathbf{p})] \tag{12a}$$

$$G(x,p) := \min_{y \in \mathcal{Y}(x,p)} g(x,y,p), \tag{12b}$$

where x are the decision variables of the first-stage problem (12a), $\mathcal{X}$ is the feasible solution set for x, and $\mathbb{E}_{\mathbf{p}}[G(x,\mathbf{p})]$ is the expectation (taken with respect to the probability distribution of the random variable $\mathbf{p}$) of the optimal value $G(x,\mathbf{p})$ of the second stage problem (12b). In (12b), $\mathcal{Y}(x,p)$ is the feasible solution set for the second-stage decision variables y, and $g(x,y,p)$ is the cost function. Notice that, for a given instance x of the first-stage variables and a given realization p of the random vector $\mathbf{p}$, (12b) is a deterministic problem.

In order to formulate the ESS sizing problem in the form (12a)-(12b), the daily demand and generation profiles are modelled as stochastic quantities by introducing the random vector $\mathbf{p}$ with elements $P_i^D(t)$, $Q_i^D(t)$, $P_i^G(t)$ and $Q_i^G(t)$ for all $i \in \mathcal{L}$ and $t \in \mathcal{T}$, where $\mathcal{T} = \{1,\dots,T\}$. The decision variables of the first-stage problem are the ESS sizes, namely $x = (E_{s_1},\dots,E_{s_m})$. Moreover, the vector containing the values $V_i(t)$, $r_s(t)$ and $b_s(t)$ for all $i \in \mathcal{L}$, $s \in \mathcal{S}$ and $t \in \mathcal{T}$, is denoted by y.

The cost function $g(x,y,p)$ of the second-stage problem is defined as a linear combination of installation costs $c(x)$ and daily operation costs $f(x,y,p)$. It takes the form

$$g(x,y,p) = c(x) + \gamma f(x,y,p), \tag{13}$$

where $\gamma \geq 0$ is a weighting parameter which trades off the two terms. Installation costs of storage are assumed to be proportional to the ESS sizes. Hence, the term $c(x)$ represents the total energy capacity corresponding to the solution x:

$$c(x) = \sum_{s \in \mathcal{S}} E_s. \tag{14}$$

The term $f(x,y,p)$ represents a weighted sum of virtual daily operation costs. These may include, for instance:

- the average total line losses per time step,

$$f_1(x,y,p) = \sum_{t \in \mathcal{T}} \sum_{i \in \mathcal{N}} P_i(t) \Delta T / T; \tag{15}$$

- the average energy exchanged by the ESSs per time step,

$$f_2(x,y,p) = \sum_{t \in \mathcal{T}} \sum_{s \in \mathcal{S}} |r_s(t)| \Delta T / T, \tag{16}$$

  which is a measure of the overall battery usage;

- the average energy exchanged at the slack bus per time step,

$$f_3(x,y,p) = \sum_{t \in \mathcal{T}} |P_1(t)| \Delta T / T, \tag{17}$$

  which is a measure of how much the considered distribution network impacts on the external grid.

With the choice (13), the two-stage stochastic optimization problem (12) can be rewritten as

$$\min_{x \in \mathcal{X}} c(x) + \gamma \mathbb{E}_{\mathbf{p}}[F(x,\mathbf{p})] \tag{18a}$$

$$F(x,p) := \min_{y \in \mathcal{Y}(x,p)} f(x,y,p). \tag{18b}$$

The first-stage problem (18a) aims at finding the ESS sizes which minimize a linear combination of installation and expected daily operation costs. The set $\mathcal{X}$ includes the constraints that all ESS sizes must be nonnegative. The second-stage problem (18b) aims at finding the optimal ESS control policy which minimizes the daily operation costs under a particular realization p of the random vector $\mathbf{p}$ and the ESS sizes defined by x. This is a multi-period AC OPF whose feasible solution set $\mathcal{Y}(x,p)$ is defined as

$$\mathcal{Y}(x,p) = \{y : (4)-(11), i \in \mathcal{L}, s \in \mathcal{S}, (i,j) \in \mathcal{E}, t \in \mathcal{T}\}, \tag{19}$$

i.e., the optimization problem is subject to constraints on ESS operation (4)–(7), power balance equations (8)-(9), and constraints (10) and (11) on voltage and apparent power. As usual in two-stage stochastic programming, ~~we set~~ $F(x,p) = \infty$ when the set $\mathcal{Y}(x,p)$ is empty. Hence, the fact that the cost in (18a) is finite for a given solution x requires that, by operating the ESSs of sizes defined by x, network constraints can be satisfied under all possible realizations of demand and generation.

2.4. Scenario-based approach to the ESS sizing problem

Solving optimization problems like (18), where uncertainty on input data is modeled by continuous, multivariate random variables, is a very hard task in general. A typical approach adopted in the literature to tackle these problems consists of discrete approximations based on scenarios [28].

In the problem at hand, a scenario is a realization p_d of the random vector $\mathbf{p}$, i.e., a particular instance of daily demand and generation profiles at network buses. Assume that a (possibly very large) set of scenarios $\mathcal{P} = \{p_1, \dots, p_D\}$ is available, and define the set of indices $\mathcal{D} = \{1, \dots, D\}$. In practical applications, scenarios can be obtained from historical data, or generated via simulation of suitable identified models [31]. Let $\{\pi_d^{\mathcal{P}}\}_{d\in\mathcal{D}}$ be the approximating probability mass function of $\mathcal{P}$ with respect to the probability distribution of $\mathbf{p}$. Moreover, define a vector of unknowns y_d with the same meaning as y in (18b), for each scenario p_d. Then, the discrete approximation of the two-stage problem (18) reads as the following (deterministic) single-stage problem:

$$\begin{aligned} J^* = \min_{x,\{y_d\}_{d\in\mathcal{D}}} \; & c(x) + \gamma \sum_{d\in\mathcal{D}} \pi_d^{\mathcal{P}} \, f(x, y_d, p_d) \\ \text{s.t.} \quad & x \in \mathcal{X}, \; y_d \in \mathcal{Y}(x, p_d), \; d \in \mathcal{D}. \end{aligned} \tag{20}$$

This approximation is justified by the fact that, if $\mathbf{p}$ were actually discrete-valued with support $\mathcal{P}$, then (18) and (20) would be equivalent thanks to the interchangeability principle [28]. In the following, the acronym ESS-OPF will be used to denote problem (20). Moreover, x^* and y_d^* will denote the values of the unknowns x and y_d at the optimum of ESS-OPF, while E_s^* is the size of the ESS at bus s corresponding to the solution x^*.

In spite of the transformation into a deterministic problem, (20) is still hard to solve for several reasons. First, the problem is an AC OPF, characterized by the intrinsic difficulties of this class of problems (e.g., nonconvexity). Second, time-coupling constraints determined by ESS dynamics, and scenario-coupling constraints represented by ESS sizes (common to all scenarios), further increase the complexity of the problem. Finally, and most importantly, a good discrete approximation requires a very large number of scenarios. This may make problem (20) practically intractable even resorting to state-of-the-art relaxation techniques for OPF problems [27, 25], due to the huge number of variables involved, calling for prohibitive memory requirements. Similar conclusions are reported in [14] for an application with a large number of scenarios.

In the next sections, an approximate solution approach for tackling problem (20), is presented. The approach is based on solving a problem similar to (20) for each scenario. Then, for the case $\gamma = 0$, an iterative algorithm is proposed to solve problem (20) at the optimum. The algorithm hinges on a metric for scenario reduction allowing one to find, provided it exists, a downsized scenario set which can replace the original set in (20), while preserving the overall optimality of the solution.

3. Approximate solution strategy

The first step of the proposed approximate solution strategy for ESS-OPF requires to solve the following problem for each scenario p_d:

$$\begin{aligned} \min_{x,y_d} \quad & c(x) + \gamma \, f(x, y_d, p_d) \\ \text{s.t.} \quad & x \in \mathcal{X}, \; y_d \in \mathcal{Y}(x, p_d). \end{aligned} \tag{21}$$

This amounts to solve a number D of multi-period OPF problems, for which solution strategies based on semidefinite programming (SDP) convex relaxations can be adopted, see, e.g., [25]. It is to remark that solving (21) is typically affordable. Moreover, the solution of the D single-scenario problems can be easily parallelized, thus reducing the overall computation time. The values of x and y_d at the optimum of problem (21) are denoted by $\widetilde{x}_d$ and $\widetilde{y}_d$, while $\widetilde{E}_{s,d}$ is the size of the ESS at bus s corresponding to the solution $\widetilde{x}_d$. Given the solutions of the single-scenario OPFs (21), the following vector of ESS sizes is defined:

$$\widetilde{x} = \max_{d\in\mathcal{D}} \widetilde{x}_d, \tag{22}$$

where the maximum is to be intended as component-wise. The size of the ESS at bus s corresponding to the solution $\widetilde{x}$ is denoted by $\widetilde{E}_s$. A feasible solution of ESS-OPF and an upper bound to its optimal cost are provided by the following theorem.

Theorem 1. The solution $(\widetilde{x}, \{\widetilde{y}_d\}_{d\in\mathcal{D}})$ is feasible for ESS-OPF. An upper bound to the optimal cost of ESS-OPF is given by

$$J_{\text{UB}} = c(\tilde{x}) + \gamma \sum_{d\in\mathcal{D}} \pi_d^{\mathcal{P}} \, f(\tilde{x}, \tilde{y}_d, p_d). \tag{23}$$

Proof. From (20), one needs to show that $\widetilde{y}_d \in \mathcal{Y}(\widetilde{x}, p_d)$ for all $d \in \mathcal{D}$. Note that the ESS sizes E_s enter the constraint sets $\mathcal{Y}(x, p_d)$ only as upper bounds in (6) and (7). Since $\widetilde{y}_d \in \mathcal{Y}(\widetilde{x}_d, p_d)$, and $\widetilde{x}$ is defined as the component-wise maximum over the set $\{\widetilde{x}_d\}_{d\in\mathcal{D}}$, it follows that $\widetilde{y}_d \in \mathcal{Y}(\widetilde{x}_d, p_d)$. This proves that $(\widetilde{x}, \{\widetilde{y}_d\}_{d\in\mathcal{D}})$ is a feasible solution to (20), and therefore

$$\begin{aligned} c(x^*) + \gamma \sum_{d\in\mathcal{D}} \pi_d^{\mathcal{P}} \, f(x^*, y_d^*, p_d) \\ \leq c(\tilde{x}) + \gamma \sum_{d\in\mathcal{D}} \pi_d^{\mathcal{P}} \, f(\tilde{x}, \tilde{y}_d, p_d), \end{aligned} \tag{24}$$

where the left-hand side of the inequality is the optimal cost of (20), whereas the right-hand side is the cost J_{UB} in (23), corresponding to the feasible solution found. This concludes the proof. □

Since the optimal cost of (20) is typically non-computable, a lower bound is derived next. The lower bound is useful to evaluate the quality of any feasible solution of (20).

Theorem 2. A lower bound to the optimal cost of ESS-OPF is given by

$$J_{\mathrm{LB}} = \sum_{d\in\mathcal{D}} \pi_d^{\mathcal{P}} \left[c(\widetilde{x}_d) + \gamma\, f(\widetilde{x}_d, \widetilde{y}_d, p_d)\right]. \tag{25}$$

Proof. The proof stems from the following inequalities:

$$\begin{aligned} c(x^*) + \gamma \sum_{d\in\mathcal{D}} \pi_d^{\mathcal{P}}\, f(x^*, y_d^*, p_d) \\ = \sum_{d\in\mathcal{D}} \pi_d^{\mathcal{P}} \left[c(x^*) + \gamma\, f(x^*, y_d^*, p_d)\right] \\ \geq \sum_{d\in\mathcal{D}} \pi_d^{\mathcal{P}} \left[c(\widetilde{x}_d) + \gamma\, f(\widetilde{x}_d, \widetilde{y}_d, p_d)\right], \end{aligned} \tag{26}$$

using the fact that $\sum_{d\in\mathcal{D}} \pi_d^{\mathcal{P}} = 1$, and the pair $(\widetilde{x}_d, \widetilde{y}_d)$ is the optimal solution of (21), which implies

$$c(\widetilde{x}_d) + \gamma\, f(\widetilde{x}_d, \widetilde{y}_d, p_d) \leq c(x^*) + \gamma\, f(x^*, y_d^*, p_d) \tag{27}$$

for all $d \in \mathcal{D}$. □

Notice that the lower bound of Theorem 2 is computable, because the values of $\widetilde{x}_d$ and $\widetilde{y}_d$ are known from the solution of (21) for each scenario.

Remark 1. A less conservative lower bound for the case $\gamma = 0$ is given by

$$J_{\mathrm{LB}}^0 = \max_{d\in\mathcal{D}} c(\widetilde{x}_d). \tag{28}$$

Indeed, since the pair (x^*, y_d^*) is feasible for (21), it holds that $c(x^*) \geq c(\widetilde{x}_d)$, and therefore

$$c(x^*) \geq \max_{d\in\mathcal{D}} c(\widetilde{x}_d) \geq \sum_{d\in\mathcal{D}} \pi_d^{\mathcal{P}}\, c(\widetilde{x}_d), \tag{29}$$

where the right-hand side of the inequality is the lower bound (25) computed for $\gamma = 0$.

4. Optimal solution via scenario reduction

When the objective of the optimization is only to minimize the total installed ESS capacity, and therefore $\gamma = 0$ in (20), an iterative procedure is proposed to solve problem (20) at the optimum, while downsizing the scenario set needed to compute the optimal solution. In the following, a solution $x \in \mathcal{X}$ is said to be feasible for scenario p_d if and only if the set $\mathcal{Y}(x, p_d)$ is nonempty. In practice, feasibility of the solution x implies that, for the given scenario p_d, it is possible to control the ESSs over $\mathcal{T}$ so that all ESS and network operation constraints are satisfied. A solution $x \in \mathcal{X}$ is feasible for problem (20) if and only if it is feasible for all scenarios.

The procedure is initialized by solving problem (21) with $\gamma = 0$ for each scenario $p_d \in \mathcal{P}$. This makes it possible to order the scenarios according to the cost $c(\widetilde{x}_d)$. In the following, $\widetilde{\mathcal{D}} = \{d_1, \ldots, d_D\}$ denotes a permutation of the set $\mathcal{D}$ such that $c(\widetilde{x}_{d_\ell}) \geq c(\widetilde{x}_{d_\kappa})$ if $\ell < \kappa$. Since $c(x^*) \geq c(\widetilde{x}_d)$ for all $d \in \mathcal{D}$ (see Remark 1), intuitively, the ordering defined by $\widetilde{\mathcal{D}}$ provides an indication of the scenarios that are most critical to determine the optimal solution x^*. This idea is exploited next to develop an effective metric for scenario reduction.

The proposed procedure for solving problem (20) at the optimum is summarized in Algorithm 1. At each iteration κ, the set of indices $\mathcal{D}_\kappa$ represents the ℓ_k scenarios p_d with the largest total ESS capacities $c(\widetilde{x}_d)$. For this scenario set, the following problem is solved:

$$\begin{aligned} \min_{x, \{y_d\}_{d\in\mathcal{D}_\kappa}} \quad & c(x) \\ \text{s.t.} \quad & x \in \mathcal{X},\ y_d \in \mathcal{Y}(x, p_d),\ d \in \mathcal{D}_\kappa. \end{aligned} \tag{30}$$

Notice that (30) coincides with (20) for $\gamma = 0$, considering a downsized scenario set in place of $\mathcal{P}$. The optimal value of x in (30) is denoted by x_κ^*. If x_κ^* is feasible for all scenarios p_d such that $d \in \mathcal{D} \setminus \mathcal{D}_\kappa$, then one can conclude its optimality for the whole scenario set $\mathcal{P}$ by virtue of the following result.

Theorem 3. *Assume $\gamma = 0$ in (20). Let $\mathcal{D}_\kappa \subset \mathcal{D}$, and denote by x_κ^* the optimal value of x in (30). If x_κ^* is feasible for all scenarios p_d such that $d \in \mathcal{D} \setminus \mathcal{D}_\kappa$, then it is optimal for (20).*

Proof. First, notice that x_κ^* is feasible for all scenarios, and hence it is feasible for problem (20). Assume that the optimal solution x^* of (20) is such that $c(x^*) < c(x_\kappa^*)$. ~~It turns out that~~ Since x^* is feasible for all scenarios, it is feasible in particular for problem (30). This leads to a contradiction, because x_κ^* minimizes the cost $c(\cdot)$ over $\mathcal{D}_\kappa$. One can therefore conclude that $c(x^*) = c(x_\kappa^*)$. □

If the feasibility test fails, the algorithm is iterated by increasing the cardinality ℓ_k of the downsized scenario set. Verifying the feasibility of a given solution x for scenario p_d amounts to check whether the set $\mathcal{Y}(x, p_d)$ is nonempty. This problem can be formulated as an OPF in the unknown y_d with constraint set $\mathcal{Y}(x, p_d)$, regardless of the considered objective function. This test can be often avoided by exploiting the solution $\widetilde{x}_d$. Indeed, if the condition $x \geq \widetilde{x}_d$ is satisfied, where the inequality has to be intended component-wise, x is feasible for scenario p_d. The proof is similar to that of Theorem 1. In the following, if $x \geq \widetilde{x}_d$, x is said to dominate $\widetilde{x}_d$.

Remark 2. A rule of thumb to define the ℓ_κ-sequence is to start with $\ell_1 = 1$. Since the solution $x_1^* = \widetilde{x}_{d_1}$ is already available for scenario p_{d_1}, one has to check only the feasibility of this solution for all other scenarios. If the feasibility test fails, one can choose ℓ_2 at the knee of the curve $c(\widetilde{x}_{d_\ell})$, $\ell = 1, \ldots, D$, compatibly with the size of the largest instance of problem (20) which can be solved.

Remark 3. Notice that Theorem 3 has a wider validity. In fact, it still holds if the set $\mathcal{D}_\kappa$ is replaced with any subset $\mathcal{D}' \subset \mathcal{D}$, no matter how $\mathcal{D}'$ is constructed. Conversely, Theorem 3 does not hold in general for $\gamma > 0$,

Algorithm 1 Scenario reduction

1: Set $\ell_0 = 0$ and $\kappa = 1$
2: Select ℓ_κ such that $\ell_{\kappa-1} < \ell_\kappa \leq D$
3: $x^*_\kappa \leftarrow$ Solve problem (30) with $\mathcal{D}_\kappa = \{d_1, \ldots, d_{\ell_\kappa}\}$
4: Check feasibility of x^*_κ for all scenarios p_d, $d \in \mathcal{D} \setminus \mathcal{D}_\kappa$
5: **if** (feasibility == **true**) **then**
6: **return** $x^* = x^*_\kappa$
7: **else**
8: $\kappa \leftarrow \kappa + 1$
9: goto 2
10: **end if**

since the values of the cost function in (20) corresponding to different scenario sets are not directly comparable.

5. Numerical results

This section demonstrates the ESS sizing procedure described in the paper, using the topology of the IEEE 37-bus test network [37], shown in Fig. 1. The lengths of the lines correspond to the original test network, while line admittances are typical of low voltage (LV) feeders. Adopted values of the resistances and reactances per unit length are shown in Table 1. They are characteristic of four different types of single-phase aerial cables. The network hosts 36 loads and 4 PV generators, whose installed power is, respectively, 10 kWp at buses 5 and 11, 9 kWp at bus 25, and 8 kWp at bus 35. Real demand and generation profiles are assigned to loads and PV generators in the test network. Available data are sampled with time step $\Delta T = 60$ min over a period of 100 days. Each day of the data set is treated as one scenario. The scenario set is denoted by $\mathcal{P} = \{p_1, \ldots, p_{100}\}$. All scenarios are considered equiprobable. In accordance with the European Norm 50160, 10% tolerance around the nominal voltage is allowed at each bus, i.e., $\underline{v}_i = 0.9$ pu and $\overline{v}_i = 1.1$ pu in (10). The bound $\overline{S}_{ij}$ in (11) is set to 50 kVA for all the lines. It is assumed that the choice of the ESSs to be deployed in the network is within a family (e.g., lithium-ion based) characterized by a coefficient $\rho_s = 1.5$ kVA/kWh in (A.3). Since the analysis presented in this section does not depend on the charging and discharging efficiencies of storage devices, η^c_s and η^d_s are set to 1 in (4). Consequently, the dynamics (4)

Table 1: Values of the cable resistance and reactance per unit length.

R [Ω/km]	X [Ω/km]
0.6410	0.0780
1.1170	0.4100
0.7200	0.3900
0.9050	0.3500

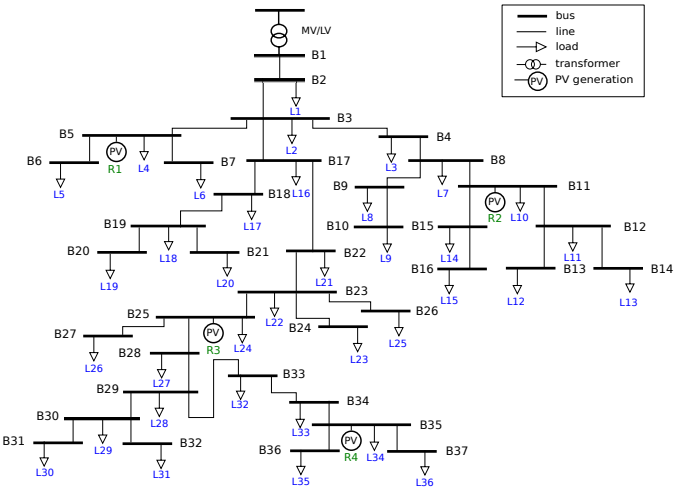

Figure 1: Test LV network with 37 buses.

of $e_s(t)$ simplifies as

$$e_s(t) = e_s(t-1) + r_s(t)\Delta T, \tag{31}$$

where the initial energy level $e_s(0)$ is set to the lower limit $\underline{E}_s = 0$. With the choice made above for the voltage bounds, the considered demand and generation profiles are such that, in the absence of ESSs, the network occasionally experiences over- and/or undervoltages. An exhaustive analysis is carried out, showing that over- and undervoltages cannot be avoided for most of the considered scenarios, by installing only one ESS of any size, and anywhere in the network. This suggests to consider two ESSs, which are placed in the network by applying the ESS siting algorithm of [17]. The algorithm returns buses 12 and 33 as the most suitable locations.

Sizing of the ESSs at buses 12 and 33 is accomplished by applying the ESS sizing procedure proposed in this paper. To this aim, the vectors Γ_s, Υ_s and Ξ_s of (7) are defined as in (A.4) for $n = 4$, corresponding to the inner approximation of the ESS capability curve with a regular octagon. In all OPF problems required by the ESS sizing procedure, the daily operation cost function $f(x, y, p)$ takes into account only the average total line losses per time step (15), i.e., $f(x, y, p) = f_1(x, y, p)$. OPF problems are tackled via the SDP convex relaxation of [25]. SDP programs are implemented through the CVX modelling package for convex optimization (version 2.1) [38], and solved via the SeDuMi solver (version 1.34) [39] on an Intel Xeon 2.4 GHz CPU with 32 GB RAM. On average, the relaxed version of the single-scenario problem (21) is solved in about 2 min. As long as it can be solved, the computation time of the SDP relaxation of the multi-scenario problem (20) grows almost quadratically with the cardinality of the set $\mathcal{D}$ [35]. For instance, it takes about three hours for a set of 10 scenarios. For all examples discussed in this section, a feasible solution to the original problem (20), (21), or (30) is reconstructed from the optimal solution of the relaxed SDP program by solving a series of

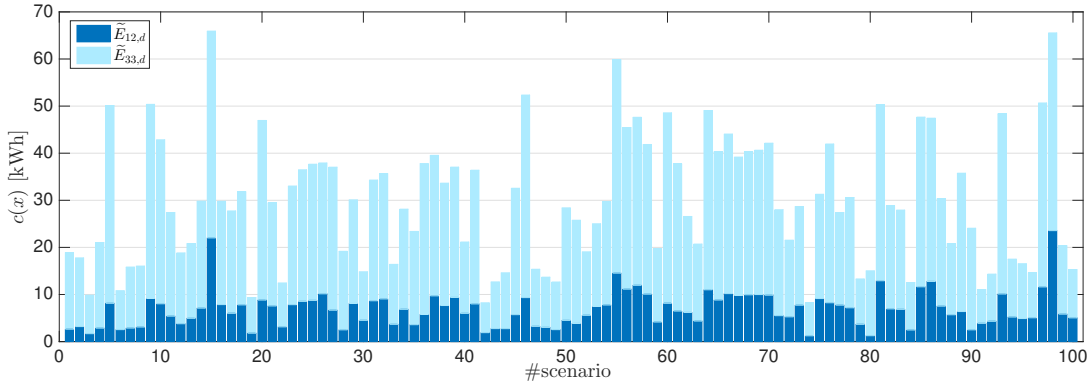

Figure 2: Results of the single-scenario problem (21) with $D = 100$ scenarios. The dark and light blue bars represent, respectively, the optimal ESS sizes $\widetilde{E}_{12,d}$ and $\widetilde{E}_{33,d}$ corresponding to each single scenario p_d.

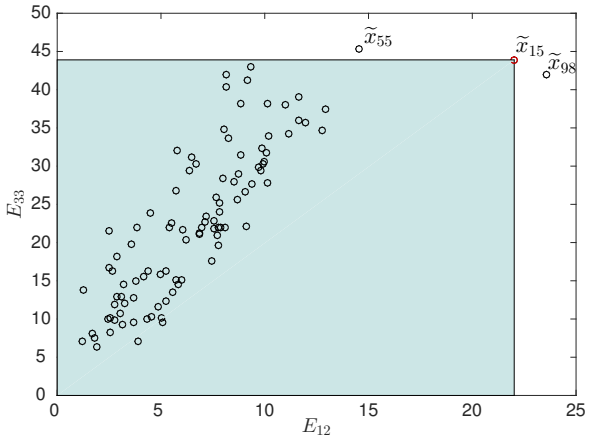

Figure 3: The solutions of the single-scenario problem (21) for each of the 100 scenarios, are represented by black circles. The colored region represents the set of solutions that are dominated by the solution of scenario p_{15} (red circle).

PFs.

5.1. Optimal solution for the case $\gamma = 0$

This section presents an application of Algorithm 1 in the case $\gamma = 0$. Problem (20) cannot be solved directly for the whole scenario set $\mathcal{P}$ composed of 100 scenarios, due to out-of-memory issues. Hence, Algorithm 1 is applied to compute the optimal solution. To initialize the algorithm, one first solves the single-scenario problem (21) for each scenario. The corresponding optimal ESS sizes $\widetilde{x}_d = \left(\widetilde{E}_{12,d}, \widetilde{E}_{33,d}\right)$, $d = 1, \ldots, 100$, are shown in the bar plot of Fig. 2, and the scatter plot of Fig. 3. In Fig. 2, for each scenario p_d, the height of the bar is the total ESS capacity $c(\widetilde{x}_d)$, while the two colors highlight the partition of $c(\widetilde{x}_d)$ between the two ESSs. Then, the scenarios are sorted according to decreasing values of $c(\widetilde{x}_d)$, ~~It turns out that~~ returning the ordered set $\widetilde{\mathcal{D}} = \{d_1, d_2, d_3, \ldots, d_{100}\} = \{15, 98, 55, \ldots, 42\}$. The lower bound (28) to the optimal cost $c(x^*)$ of (20), is $c(\widetilde{x}_{15}) = 65.92$ kWh, while the upper bound to $c(x^*)$ is $c(\widetilde{x}) = 68.84$ kWh, with $\widetilde{x}$ given by (22). In the first iteration of Algorithm 1, $\mathcal{D}_1 = \{15\}$ is considered. Since $x_1^* = \widetilde{x}_{15}$, one has to check only whether the solution $\widetilde{x}_{15}$ is feasible for all other scenarios. The gray region in Fig. 3 represents the set of solutions that are dominated by $\widetilde{x}_{15}$, and one can therefore conclude that $\widetilde{x}_{15}$ is feasible for all scenarios, except p_{55} and p_{98}. For these two scenarios, a feasibility check has to be accomplished, and it turns out that the test fails for scenario p_{55}. Hence, Algorithm 1 does not stop, and a further iteration is required.

In the second iteration of the algorithm, $\mathcal{D}_2 = \{15, 98\}$ is considered, i.e., $\mathcal{D}_2$ is formed by the two scenarios featuring the largest total ESS capacities. Problem (30) is solved, and returns the solution x_2^*. The feasibility check of x_2^* again fails for scenario p_{55}, and a third iteration of the algorithm is required.

In the third iteration, scenario p_{55} is added, being the third element according to the ordered set $\widetilde{\mathcal{D}}$. Problem (30) is solved with $\mathcal{D}_3 = \{15, 98, 55\}$, returning the solution x_3^*, which is feasible for all scenarios. Hence, Algorithm 1 terminates with the optimal solution $x^* = x_3^*$ for problem (20).

The three iterations of the algorithm are summarized in Table 2, where $E_{s,\kappa}^*$ is the ESS size at bus s corresponding to the solution x_κ^*. Notice that the algorithm generates a sequence of lower bounds converging to the optimal cost $c(x^*)$. A graphical representation of the algorithm iterations is provided in Fig. 4, also showing that

Table 2: Summary of the iterations of Algorithm 1. ESS sizes are expressed in kWh.

κ	$\mathcal{D}_\kappa$	$E_{12,\kappa}^*$	$E_{33,\kappa}^*$	$c(x_\kappa^*)$
1	$\{15\}$	22.02	43.90	65.92
2	$\{15, 98\}$	25.08	42.17	67.35
3	$\{15, 55, 98\}$	25.78	41.76	67.54

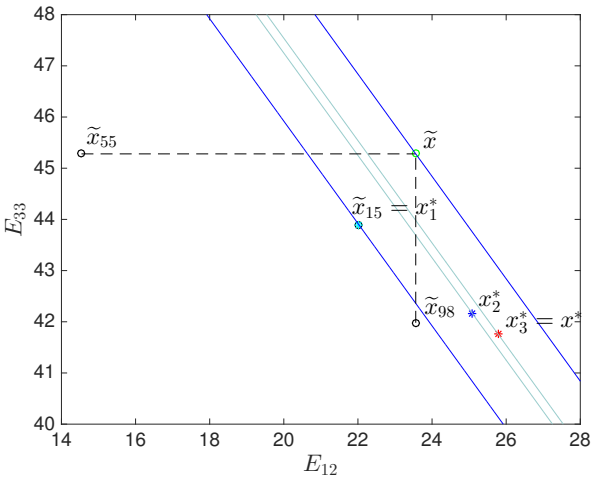

Figure 4: Graphical representation of the ESS sizing procedure of Section 4, including the computation of lower and upper bounds to the optimal cost $c(x^*)$, and the iterations of Algorithm 1. The oblique lines represent level curves of the cost function $c(x)$.

$\widetilde{E}_{12} = \widetilde{E}_{12,98}$ and $\widetilde{E}_{33} = \widetilde{E}_{33,55}$.

Remark 4. In the proposed application of Algorithm 1, only one scenario is added at each iteration. This is done for illustrative purposes. In practice, since in the first iteration of the algorithm the feasibility check fails only for scenario p_{55}, one could argue that this scenario is critical, and decide to include it in the set $\mathcal{D}_2$. To do this, one has to choose $\ell_2 = 3$ in Algorithm 1, and hence $\mathcal{D}_2 = \{15, 98, 55\}$. In this way, the algorithm would stop in the second iteration.

5.2. Approximate solutions for the case $\gamma > 0$

The aim of this section is to validate the bounds (23) and (25) on the optimal cost J^*, using instances of problem (20) that can be computationally solved. In particular, the gap between the upper bound $J_{\rm UB}$ and both the optimal cost J^* and the lower bound $J_{\rm LB}$, is evaluated. To this purpose, the following percent errors are considered:

$$\eta^* = \frac{J_{\rm UB} - J^*}{J_{\rm UB}}\% \tag{32}$$

$$\eta^w = \frac{J_{\rm UB} - J_{\rm LB}}{J_{\rm UB}}\%. \tag{33}$$

The 100 available scenarios are partitioned into 10 non-overlapping groups $\mathcal{P}_1, \ldots, \mathcal{P}_{10}$ of 10 scenarios each. For each group, J^* is computed by solving the multi-scenario problem (20) for three different values of γ, namely $\gamma = 100$, 500, and 1000. Then, in order to compute the bounds $J_{\rm LB}$ and $J_{\rm UB}$, 10 single-scenario problems (21) are solved for each value of γ. Results are shown in Table 3. As expected, there always holds $J_{\rm LB} \le J^* \le J_{\rm UB}$. Percent errors (32) and (33) are averaged over the 10 groups of problems. ~~It turns out that,~~ In terms of mean values, $\eta^w = 21.43\%$ and $\eta^* = 12.75\%$ for $\gamma = 100$, $\eta^w = 6.65\%$ and $\eta^* = 3.42\%$ for $\gamma = 500$, and $\eta^w = 3.78\%$ and $\eta^* = 2.05\%$ for $\gamma = 1000$. This implies that η^* is typically a fraction of η^w ranging from 0.5 to 0.6. Moreover, it can be noticed that the values of η^* and η^w decrease as γ grows. This is consistent with the intuition that the lower bound $J_{\rm LB}$ tends to the upper bound $J_{\rm UB}$ when greater weight is given to the operation cost $f(\cdot)$ in (13), as compared to the installation cost $c(\cdot)$.

It is stressed that, as discussed at the end of Section 2.4, problem (20) cannot be computationally solved in practical applications with a large number of scenarios, and therefore η^* cannot be evaluated, in general. On the other hand, η^w can be typically computed, and provides the decision maker with a worst-case indication (i.e., in the case J^* would be actually equal to $J_{\rm LB}$) about the optimality gap of the feasible solution found via Theorem 1. For instance, in our application, problem (20) cannot be solved with 100 scenarios due to out-of-memory issues, whereas the 100 single-scenario problems (21) needed to compute the bounds $J_{\rm LB}$ and $J_{\rm UB}$, are solved in about 200 min (without parallelization). Lower and upper bounds are shown in Table 4 for $\gamma = 100$, 500, and 1000. The corresponding percent errors η^w are 31.81% for $\gamma = 100$, 8.47% for $\gamma = 500$, and 4.25% for $\gamma = 1000$. This confirms the decrease of η^w as γ grows.

5.3. Comparison of scenario reduction techniques

An important issue in scenario reduction is concerned with the quality of the reduction process, which is to be measured in terms of the solution to the original problem. In other words, a good reduction process provides a scenario subset yielding a solution which is close, and possibly equal, to the solution obtained with the whole scenario set [31].

In this section, the scenario reduction technique of Section 4, based on ordering the scenarios according to the optimal cost of the single-scenario problem (21), is compared with a scenario reduction technique based on the notion of probability distance [33]. A probability distance allows one to quantify the closeness of two different scenario sets that represent the same stochastic process. The idea is to preserve as much as possible the stochastic information of the original set in the downsized scenario set. For a fixed cardinality N of the downsized scenario set, the technique in [33] selects N representative scenarios from the original scenario set $\mathcal{P}$, based on the Kantorovich distance. The interested reader is referred to [31, Chap. 3] for the implementation of the technique adopted in this paper.

Let $N = 10$. As described in Section 4, a downsized scenario set $\mathcal{P}_o$ is constructed by selecting the first N scenarios of $\mathcal{P}$ according to the ordering induced by $\widetilde{\mathcal{D}}$. A different downsized scenario set $\mathcal{P}_p$ of cardinality N is obtained by applying the scenario reduction technique of [33]. Then, problem (20) is solved for both scenario sets $\mathcal{P}_o$ and $\mathcal{P}_p$. Figure 5 shows the results obtained using $\mathcal{P}_o$. ~~It turns out that~~ The solution found with the downsized set $\mathcal{P}_o$ is equal to the optimal solution of problem (20) for the whole set $\mathcal{P}$. On the other hand, Fig. 6 shows the results

Table 3: Optimal cost J^* of problem (20) for different values of γ, and corresponding bounds J_{LB} and J_{UB} (in kWh). Each row refers to a different scenario set composed of 10 scenarios.

	$\gamma = 100$			$\gamma = 500$			$\gamma = 1000$		
	J_{LB}	J^*	J_{UB}	J_{LB}	J^*	J_{UB}	J_{LB}	J^*	J_{UB}
$\mathcal{P}_1$	76.84	91.53	103.74	260.14	272.39	277.97	478.42	489.92	494.08
$\mathcal{P}_2$	89.41	101.35	125.68	309.30	330.33	335.39	574.63	594.88	597.91
$\mathcal{P}_3$	82.87	88.91	93.25	284.99	287.72	291.68	528.05	530.96	535.11
$\mathcal{P}_4$	86.65	91.81	96.56	297.42	299.58	304.25	552.27	554.57	559.20
$\mathcal{P}_5$	77.94	88.91	110.13	272.62	285.79	299.41	501.86	514.66	533.67
$\mathcal{P}_6$	100.16	110.93	135.73	339.21	352.96	391.08	629.20	641.83	684.84
$\mathcal{P}_7$	97.32	102.12	108.80	322.60	327.61	331.43	597.26	601.30	604.20
$\mathcal{P}_8$	76.75	82.59	95.10	265.90	271.45	278.35	490.88	496.03	502.94
$\mathcal{P}_9$	91.13	101.20	108.63	311.26	319.22	323.46	577.77	584.65	587.73
$\mathcal{P}_{10}$	82.80	100.61	130.90	284.87	305.26	333.83	525.95	546.38	576.91

obtained using $\mathcal{P}_p$. The solution found with the downsized set $\mathcal{P}_p$ is infeasible for at least three scenarios in $\mathcal{P} \setminus \mathcal{P}_p$ (those corresponding to the three black circles above the gray line in Fig. 6). Moreover, the total ESS capacity of this solution is about 25% less than the minimum required to guarantee feasibility over the whole scenario set $\mathcal{P}$.

The results of this section confirm, as also reported in [34], that metrics based on probability distance criteria, are not suitable to downsize the scenario set for the ESS sizing problem (20). Vice versa, the scenario reduction technique of this paper turns out to be extremely effective, being derived by exploiting the structure of problem (20).

6. Discussion

The significance of the numerical results presented in Section 5 does not lie in the particular test network and data used. Starting from an optimization problem which is of strong interest in applications, but cannot be solved directly due to computational issues, it is shown that bounds on the optimal cost, and a good feasible solution of that problem, can be obtained by applying a suitable decomposition approach. Moreover, if the objective is to minimize the total installed storage capacity, the proposed iterative procedure of Algorithm 1 allows one to compute the actual optimal solution. In this respect, these contributions represent an important bridge from theory to application.

Table 4: Bounds J_{LB} and J_{UB} (in kWh) of the optimal cost J^* of problem (20) for a scenario set composed of 100 scenarios. Each row corresponds to a different value of γ.

γ	J_{LB}	J_{UB}
100	86.19	126.40
500	294.83	322.13
1000	545.73	569.94

The aforementioned iterative procedure is based on a metric for scenario reduction, which exploits the structure of the multi-scenario problem. In the presented numerical results, this *ad hoc* metric is shown to be extremely effective for the problem at hand compared to standard clustering methods, typically adopted in the literature on scenario-based approaches.

Finally, although the main focus of the paper is on the use of ESSs for voltage support, ESSs can be adopted to provide different services to the grid, such as peak load shaving, load curve smoothing, and reduction of DG curtailment. The more services the ESSs simultaneously provide, the more advantageous their installation is from the economic point of view. If ESS sizing has to take into account the provision of multiple services, additional network operation constraints should be included in the optimization problems, as well as new terms could be added to the cost function $f(x, y, p)$ in (13). As a matter of fact, these changes do not affect the ESS operation constraints. Since all the results obtained in the paper derive from the structure of the constraints (6)-(7), where the ESS sizes E_s enter as upper bounds, it can be concluded that the proposed technique can be readily generalized to sizing problems where ESSs provide multiple services.

7. Conclusions and future work

This paper addressed the problem of finding the optimal sizes of energy storage systems in distribution networks. A two-stage stochastic programming formulation was adopted to accommodate uncertainty on future demand and generation. Then, a scenario-based discrete approximation of the two-stage problem, in the form of a multi-scenario optimal power flow, was derived. Since the latter problem rapidly becomes intractable as the number of scenarios grows, a procedure to compute a feasible solution of the multi-scenario problem was proposed. This procedure provides also upper and lower bounds to the

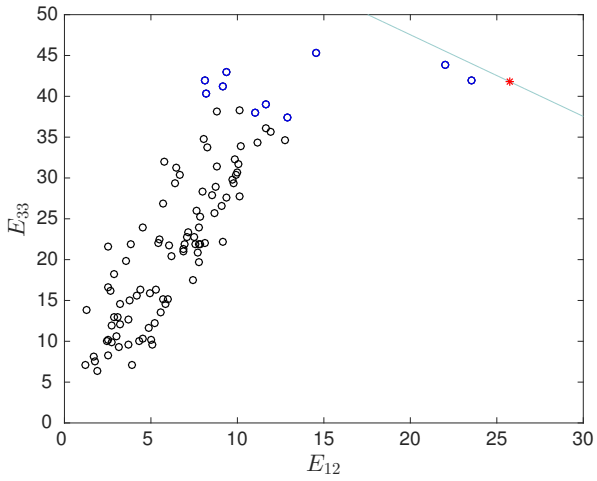

Figure 5: Results of scenario reduction based on Algorithm 1. The blue circles correspond to the first ten scenarios according to the ordering induced by $\widetilde{\mathcal{D}}$, and the red star represents the solution obtained by solving problem (20) for this downsized scenario set.

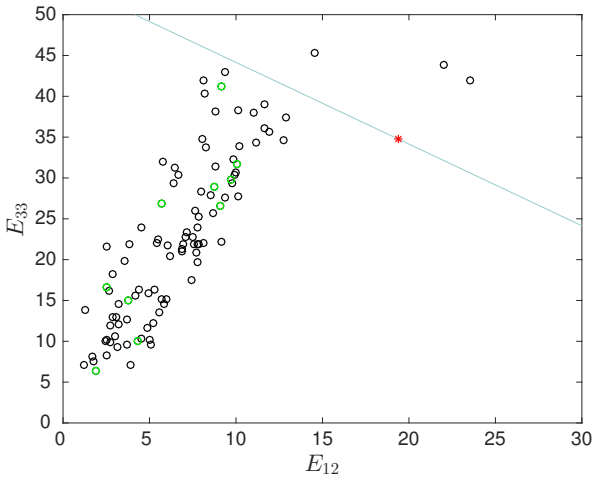

Figure 6: Results of scenario reduction based on [33]. The green circles correspond to the ten scenarios selected based on a probability distance criterion, and the red star represents the solution obtained by solving problem (20) for this downsized scenario set.

optimal cost of the multi-scenario problem. Moreover, for the case when the objective is to minimize the total installed storage capacity, a computationally tractable, iterative procedure was devised to solve the corresponding optimization problem. The proposed bounds and procedure were validated on the topology of the IEEE 37-bus test network. Numerical results confirmed both the theoretical bounds, and the convergence of the iterative algorithm to the optimal solution of the multi-scenario problem. Finally, a comparison with a scenario reduction technique based on a probability distance criterion, was carried out, showing that the metric for scenario reduction proposed in the paper is more effective for the purpose of the considered sizing problem.

In this paper, the sizing problem was addressed in a worst-case sense, since power flow and network constraints had to be fulfilled under all scenarios. Future work will focus on a more general setting, where hard constraints are replaced or complemented with probabilistic constraints.

Appendix A. Linearized ESS capability curve

The ESS capability curve is translated into the following constraint on the apparent power delivered by the ESS at time t:

$$r_s(t)^2 + b_s(t)^2 \leq \overline{S}_s^2, \tag{A.1}$$

where $\overline{S}_s$ is a given upper bound for the ESS at bus s. The circular region defined by (A.1) is linearized via a polygonal inner approximation defined by (7). The vectors Γ_s, Υ_s and Ξ_s in (7) are derived next when the approximation is a regular polygon of $2n$ sides, $n = 2, 3, \ldots$, with a vertex in the point $(\overline{S}_s, 0)$. The case $n = 4$ is shown in Fig. A.7.

Let $\theta = \frac{\pi}{n}$, and $\theta_k = k\theta$, with k an integer number. The vertices of the regular polygon are the points $P_k = (\overline{S}_s \cos\theta_k, \overline{S}_s \sin\theta_k)$, $k = 0, 1, \ldots, 2n-1$. Let L_k be the line passing through the points P_k and P_{k+1} (with $P_{2n} = P_0$), and define $\mathcal{H}_k$ the half-plane on the side of the line L_k which contains the origin. The half-plane $\mathcal{H}_k$ is defined by the linear inequality

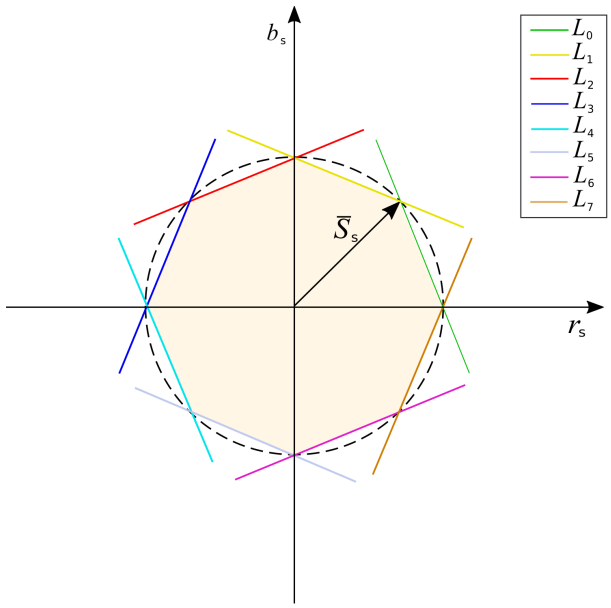

Figure A.7: Inner approximation of a circular region with a regular polygon of 8 sides ($n = 4$).

$$(\sin\theta_{k+1} - \sin\theta_k)\, r_s - (\cos\theta_{k+1} - \cos\theta_k)\, b_s \leq \overline{S}_s \sin(\theta). \tag{A.2}$$

In order to model the possible dependence of power ratings on energy ratings for a given storage technology [18], the upper bound $\overline{S}_s$ is assumed to be proportional to the ESS size E_s. Hence,

$$\overline{S}_s = \rho_s E_s, \tag{A.3}$$

$$\Gamma_s = \begin{bmatrix} \sin\theta_1 - \sin\theta_0 \\ \sin\theta_2 - \sin\theta_1 \\ \vdots \\ \sin\theta_{2n} - \sin\theta_{2n-1} \end{bmatrix}, \quad \Upsilon_s = - \begin{bmatrix} \cos\theta_1 - \cos\theta_0 \\ \cos\theta_2 - \cos\theta_1 \\ \vdots \\ \cos\theta_{2n} - \cos\theta_{2n-1} \end{bmatrix}, \quad \Xi_s = - \left.\begin{bmatrix} \rho_s \sin\theta \\ \rho_s \sin\theta \\ \vdots \\ \rho_s \sin\theta \end{bmatrix}\right\} 2n \tag{A.4}$$

where ρ_s is fixed, and characteristic of the storage technology adopted at bus s. Since the polygon is finally defined by the intersection of the half-planes $\mathcal{H}_k$ in (A.2), the vectors Γ_s, Υ_s and Ξ_s take the form in (A.4).

References

[1] P. Wang, D. H. Liang, J. Yi, P. F. Lyons, P. J. Davison, P. C. Taylor, Integrating electrical energy storage into coordinated voltage control schemes for distribution networks, IEEE Transactions on Smart Grid 5 (2) (2014) 1018–1032.

[2] F. A. Viawan, A. Sannino, J. Daaldera, Voltage control with on-load tap changers in medium voltage feeders in presence of distributed generation, Electric Power Systems Research 77 (10) (2007) 1314–1322.

[3] C. Long, L. F. Ochoa, Voltage control of PV-rich LV networks: OLTC-fitted transformer and capacitor banks, IEEE Transactions on Power Systems 31 (5) (2016) 4016–4025.

[4] C. Long, J. Wu, T. Lee, N. Jenkins, Optimal operation of soft open points in medium voltage electrical distribution networks with distributed generation, Applied Energy 184 (2016) 427–437.

[5] P. M. S. Carvalho, P. F. Correia, L. A. F. M. Ferreira, Distributed reactive power generation control for voltage rise mitigation in distribution networks, IEEE Transactions on Power Systems 23 (2) (2008) 766–772.

[6] S. Chu, A. Majumdar, Opportunities and challenges for a sustainable energy future, Nature 488 (7411) (2012) 294–303.

[7] X. Luo, J. Wang, M. Dooner, J. Clarke, Overview of current development in electrical energy storage technologies and the application potential in power system operation, Applied Energy 137 (2015) 511–536.

[8] M. Aneke, M. Wang, Energy storage technologies and real life applications - a state of the art review, Applied Energy 179 (2016) 350–377.

[9] H. Zhao, Q. Wua, S. Huc, H. Xu, C. N. Rasmussen, Review of energy storage system for wind power integration support, Applied Energy 137 (2015) 545–553.

[10] M. Zidar, P. S. Georgilakis, N. D. Hatziargyriou, T. Capuder, D. Škrlec, Review of energy storage allocation in power distribution networks: applications, methods and future research, IET Generation, Transmission & Distribution 10 (3) (2016) 645–652.

[11] D. Q. Hung, N. Mithulananthan, R. Bansal, An optimal investment planning framework for multiple distributed generation units in industrial distribution systems, Applied Energy 124 (2014) 62–72.

[12] J. Sardi, N. Mithulananthan, M. Gallagher, D. Q. Hung, Multiple community energy storage planning in distribution networks using a cost-benefit analysis, Applied Energy 190 (2017) 453–463.

[13] M. Nick, R. Cherkaoui, M. Paolone, Optimal allocation of dispersed energy storage systems in active distribution networks for energy balance and grid support, IEEE Transactions on Power Systems 29 (5) (2014) 2300–2310.

[14] M. Nick, R. Cherkaoui, M. Paolone, Optimal siting and sizing of distributed energy storage systems via alternating direction method of multipliers, International Journal of Electrical Power & Energy Systems 72 (2015) 33–39.

[15] O. Babacan, W. Torre, J. Kleissl, Siting and sizing of distributed energy storage to mitigate voltage impact by solar PV in distribution systems, Solar Energy 146 (2017) 199–208.

[16] M. Motalleb, E. Reihani, R. Ghorbani, Optimal placement and sizing of the storage supporting transmission and distribution networks, Renewable Energy 94 (2016) 651–659.

[17] A. Giannitrapani, S. Paoletti, A. Vicino, D. Zarrilli, Optimal allocation of energy storage systems for voltage control in LV distribution networks, IEEE Transactions on Smart Grid 8 (6) (2017) 2859–2870.

[18] C. Thrampoulidis, S. Bose, B. Hassibi, Optimal placement of distributed energy storage in power networks, IEEE Transactions on Automatic Control 61 (2) (2016) 416–429.

[19] S. Wogrin, D. F. Gayme, Optimizing storage siting, sizing, and technology portfolios in transmission-constrained networks, IEEE Transactions on Power Systems 30 (6) (2015) 3304–3313.

[20] M. Ghofrani, A. Arabali, M. Etezadi-Amoli, M. S. Fadali, A framework for optimal placement of energy storage units within a power system with high wind penetration, IEEE Transactions on Sustainable Energy 4 (2) (2013) 434–442.

[21] E. Grover-Silva, R. Girard, G. Kariniotakis, Optimal sizing and placement of distribution grid connected battery systems through an SOCP optimal power flow algorithm, Applied Energy (2017). In press.

[22] P. Fortenbacher, A. Ulbig, G. Andersson, Optimal placement and sizing of distributed battery storage in low voltage grids using receding horizon control strategies, IEEE Transactions on Power Systems (2017). In press.

[23] K. Baker, G. Hug, X. Li, Energy storage sizing taking into account forecast uncertainties and receding horizon operation, IEEE Transactions on Sustainable Energy 8 (1) (2017) 331–340.

[24] Y. Tang, S. H. Low, Optimal placement of energy storage in distribution networks, IEEE Transactions on Smart Grid 8 (6) (2017) 3094–3103.

[25] J. Lavaei, S. H. Low, Zero duality gap in optimal power flow problem, IEEE Transactions on Power Systems 27 (1) (2012) 92–107.

[26] D. Gayme, U. Topcu, Optimal power flow with large-scale storage integration, IEEE Transactions on Power Systems 28 (2) (2013) 709–717.

[27] S. Low, Convex relaxation of optimal power flow – Part I: Formulations and equivalence, IEEE Transactions on Control of Network Systems 1 (1) (2014) 15–27.

[28] A. Shapiro, D. Dentcheva, A. Ruszczyński, Lectures on Stochastic Programming: Modeling and Theory, 2nd Edition, MOS-SIAM Series on Optimization, Society for Industrial and Applied Mathematics, Philadelphia, PA, USA, 2014.

[29] A. S. A. Awad, T. H. M. EL-Fouly, M. M. A. Salama, Optimal ESS allocation for benefit maximization in distribution networks, IEEE Transactions on Smart Grid 8 (4) (2017) 1668–1678.

[30] A. Kargarian, G. Hug, J. Mohammadi, A multi-time scale co-optimization method for sizing of energy storage and fast-ramping generation, IEEE Transactions on Sustainable Energy 7 (4) (2016) 1351–1361.

[31] A. J. Conejo, M. Carrión, J. M. Morales, Decision Making Under Uncertainty in Electricity Markets, Int. Series in Operations Research & Management Science, Springer, New York, NY, 2010.

[32] G. Papaefthymiou, D. Kurowicka, Using copulas for modeling stochastic dependence in power system uncertainty analysis, IEEE Transactions on Power Systems 24 (1) (2009) 40–49.

[33] J. Dupačová, N. Gröwe-Kuska, W. Römisch, Scenario reduction in stochastic programming, Mathematical Programming 95 (3) (2003) 493–511.

[34] M. Bucciarelli, A. Giannitrapani, S. Paoletti, A. Vicino,

D. Zarrilli, Energy storage sizing for voltage control in LV networks under uncertainty on PV generation, in: Proc. of 2nd Int. Forum on Research and Technologies for Society and Industry, Bologna, Italy, 2016, pp. 1–6.

[35] M. Bucciarelli, A. Giannitrapani, S. Paoletti, A. Vicino, D. Zarrilli, Sizing of energy storage systems considering uncertainty on demand and generation, IFAC-PapersOnLine 50 (1) (2017) 8861–8866.

[36] J. A. Momoh, Electric Power System Applications of Optimization, 2nd Edition, CRC Press, Boca Raton, FL, 2009.

[37] W. Kersting, Radial distribution test feeders, IEEE Transactions on Power Systems 6 (3) (1991) 975–985.

[38] M. Grant, S. Boyd, CVX: Matlab software for disciplined convex programming, version 2.1, [Online]. Available: `http://cvxr.com/cvx` (accessed Nov. 21, 2017) (Mar 2017).

[39] J. Sturm, Using SeDuMi 1.02, A Matlab toolbox for optimization over symmetric cones, Optimization Methods & Software 11 (1-4) (1999) 625–653.